J. Fluid Mech. (2009), *vol.* 635, *pp.* 189–206.
doi:10.1017/S002211200900771X

Viscous simulation of shock-reflection hysteresis in overexpanded planar nozzles

E. SHIMSHI, G. BEN-DOR AND A. LEVY†

Pearlstone Center for Aeronautical Engineering Studies, Department of Mechanical Engineering, Ben-Gurion University of the Negev, Beer Sheva, Israel

(Received 20 October 2008; revised 8 April 2009; accepted 8 April 2009)

A computational fluid dynamics simulation of the flow in an overexpanded planar nozzle shows the existence of Mach-reflection hysteresis inside the nozzle. Previous simulations have dealt only with the flow outside the nozzle and thus concluded that the hysteresis phenomenon takes place outside the nozzle even when viscous effects are introduced. When including the geometry of the nozzle in the simulation it becomes evident that flow separation will occur before the transition from regular to Mach reflection for all relevant Mach numbers. The simulation reveals complex changes in the flow structure as the pressure ratio between the ambient and the jet is increased and decreased. The pressure along the nozzle wall downstream of the separation point is found to be less than the ambient pressure, and a modification of the Schilling curve fit is suggested for cases of extensive flow separation.

1. Introduction

The study of supersonic jets is of great importance in many engineering applications, especially in the aeronautic and space industry. In most cases the ambient conditions into which the supersonic jet enters are not matched to the jet static pressure, and thus shock or expansion waves appear and may cause detrimental effects on the performance of the jet.

In planar overexpanded nozzle flow, a supersonic jet issuing from the nozzle outlet negotiates the pressure difference between the jet static pressure and the ambient conditions by creating an oblique shock that starts at the nozzle lip and is directed towards the symmetry plane. This incident shock (IS) can be reflected either as a regular reflection (RR) or as a Mach reflection (MR) depending on the Mach number, ratio of specific heats and the pressure ratio between the jet and the ambient. The use of the pressure ratio between the ambient pressure and the jet static pressure at a specific Mach number ($JPR = P_{amb}/P_{jet}$) is more appropriate in this context than the more familiar nozzle pressure ratio (NPR), as it gives a measure of the overexpansion degree (i.e. $JPR = 1$ is a perfectly expanded jet). The flow structure from an overexpanded nozzle is similar to the case of supersonic flow between wedges in which, for a given flow Mach number, the type of reflection is dictated by the wedge angle (figure 1).

Shock-reflection hysteresis in the flow between wedges has been studied theoretically (Li & Ben-Dor 1997; Schotz *et al.* 1997), numerically (Vuillon, Zeitoun & Ben-Dor 1995) and experimentally (Chpoun *et al.* 1995; Skews 1997; Ivanov *et al.* 2001) during the past couple of decades. The possibility of such a phenomenon was first suggested

† Email address for correspondence: avi@bgu.ac.il

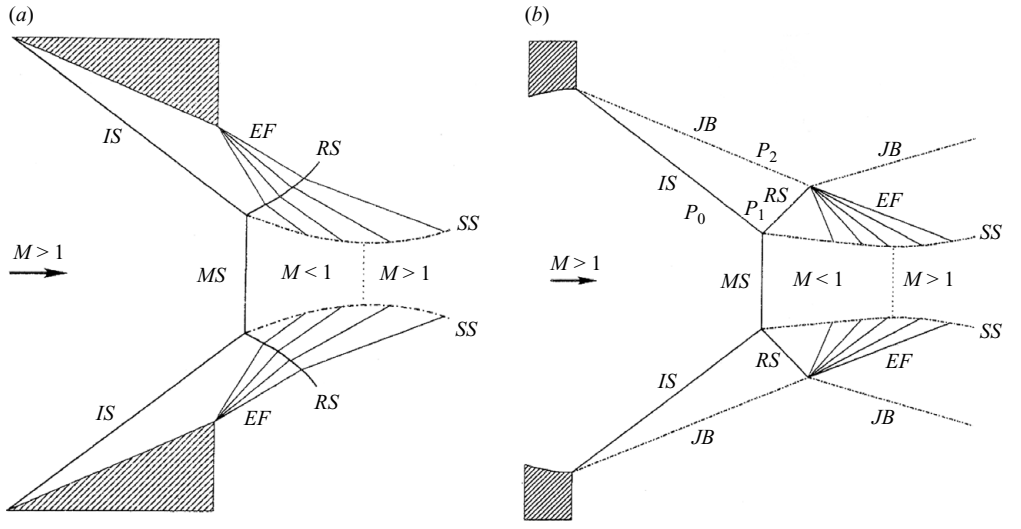

FIGURE 1. Similarity in flow structure between (*a*) wedge flow and (*b*) nozzle flow: *IS*, incident shock; *RS*, reflected shock; *MS*, Mach stem; *JB*, jet boundary; *EF*, expansion fan; *SS*, slipstream (Hadjadj 2004).

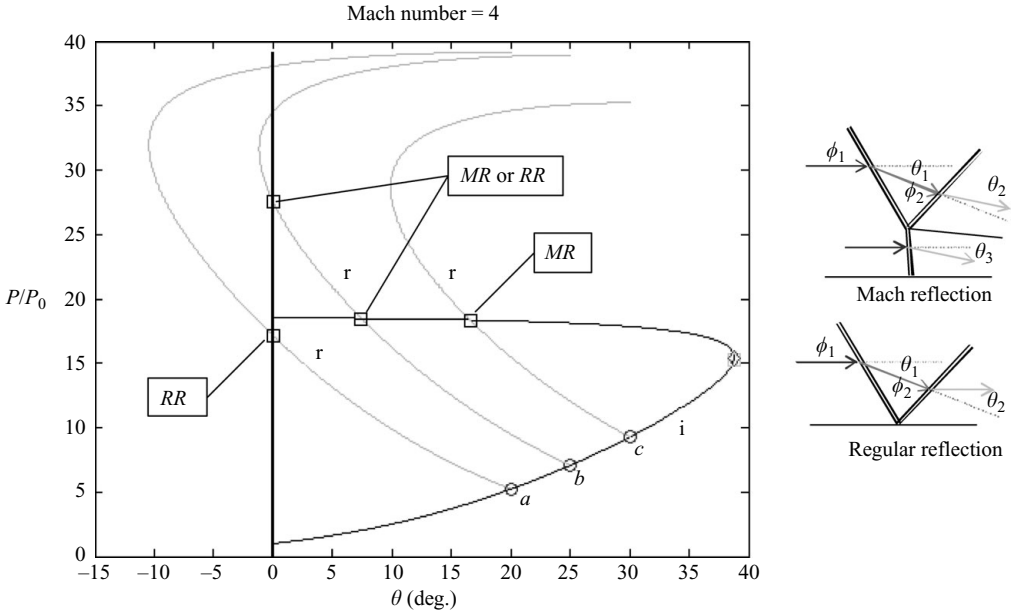

FIGURE 2. Shock polar of incident (i) and reflected (r) shocks showing three possible solutions: (*a*) only *RR*; (*b*) both *RR* and *MR*; and (*c*) only *MR*.

by Hornung, Oertel & Sandeman (1979) and was based on the occurrence of a dual-solution domain in the two-shock and three-shock theories developed by von Neumann in the mid 1940s. Experimental verification was first provided by Chpoun *et al.* (1995) in a wind-tunnel experiment.

A pressure-deflection shock polar showing the incident and reflected shocks can be used to visualize the dual-solution domain (figure 2). The i-polar represents all

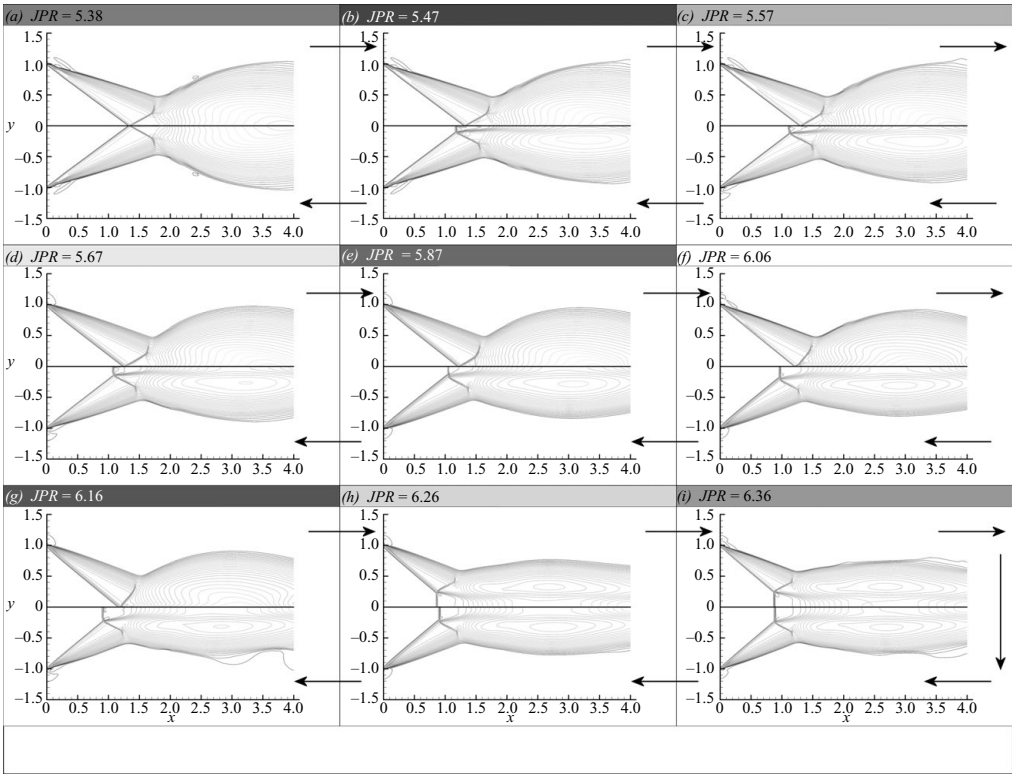

FIGURE 3. Mach isolines of hysteresis loop in an $M = 3.67$ jet. Each frame shows reflection at the same JPR; the top panel is for increased JPR and the bottom panel for decreased JPR.

possible states of flow after the incident shock; the r-polars represent all possible states of flow after the reflected shock. In case 'a' the reflected shock can deflect the flow back to parallel flow as required in RR, while in case 'c' such a deflection is not possible, and thus MR is the only solution. In case 'b' both RR and MR are possible, and the resulting flow structure depends on the previous condition, i.e. $a \rightarrow b \Rightarrow RR$, while $c \rightarrow b \Rightarrow MR$.

The occurrence of this phenomenon in the outlet of an overexpanded converging–diverging nozzle has only a few numerical references (Kudryavtsev *et al.* 2002; Hadjadj 2004), and no experimental work on it has been done.

It should be noted that although the flow pattern from an overexpanded axisymmetric jet appears to be very similar to the flow from a planer nozzle, there is a distinct difference between them. In the case of axisymmetric flow, a regular reflection is impossible (Courant & Friedrichs 1948; Ralov 1990; Molder *et al.* 1997), and thus no hysteresis can occur.

1.1. *Simulation of shock hysteresis in nozzle outlets*

Inviscid numerical simulation of an overexpanded jet at the outlet of the nozzle was preformed (Shimshi, Ben-Dor & Levy 2008) by a piecewise change in the ambient pressure from the state in which only RR is possible to the state in which only MR is possible and vice versa (figure 3). The flow conditions in the inlet of the computational domain were set by specifying the stagnation and static pressures, which dictate the

Mach number by the isentropic relation

$$\frac{p}{p_0} = \left(1 + \frac{\gamma - 1}{2} M^2\right)^{-\frac{\gamma}{\gamma - 1}}.$$

These conditions remained constant throughout the simulation.

The simulation (figure 3) shows a significant range of pressure ratios in which the hysteresis is evident (frames in which the top and bottom parts are different). The bounds of the dual-solution domain were in fair agreement with detachment criterion for the *RR* and the von Neumann criterion for the *MR* (Neumann 1943). The discrepancy from analytic results can be attributed to two numerical artefacts: the piecewise change in the ambient pressure conditions can lead to transient instability in the flow, which triggers early transition between the reflection types, and the inability of the numeric code to resolve a Mach stem that is less than three cells high results in premature transition from *MR* to *RR*. The slight difference in the location of the Mach stem between the two simulations at $JPR = 6.26$ (figure 3*h*) is yet to be understood.

A similar simulation, which included viscous effects, showed little difference from the inviscid one. This is in agreement with the work of Hadjadj (2004), which concludes that the shock-cell structure is predominantly inviscid and thus that the hysteresis is an inviscid process.

However, this type of simulation is somewhat unrealistic, as it does not include the nozzle, which produces the jet in the domain of the numeric computation.

1.2. *Flow separation in nozzle flow*

In order to produce a uniform and parallel flow at a desired Mach number in the outlet of a converging–diverging nozzle, a specific nozzle contour is required. Such a contour may be calculated by the method of characteristics (MoC). Sivells (1978) nozzle design code for wind tunnels is a very comprehensive program that uses several techniques in order to compute a nozzle contour, which will produce the desired jet, taking into account the curvature of the sonic line at the throat, the centreline distribution of Mach numbers and the boundary-layer growth along the wall. With the aid of this code, a planar nozzle contour was constructed with the following characteristics:

(i) Exit-to-throat area ratio $AR = 8$
(ii) Throat radius of curvature ratio $r_c = 16$
(iii) Exit Mach number $M_0 = 3.67$
(iv) Fluid properties of air $\gamma = 1.4$
(v) No radial-flow region
(vi) No boundary-layer correction

The resulting contour was used to build the computational domain. The inviscid computational fluid dynamics (CFD) computation shows excellent agreement with the MoC calculations (figure 4) even though the nozzle was overexpanded to a *JPR* of 6. When viscous terms were included in the numeric simulation, extensive flow separation was observed. From the point of separation on the wall, the incident shock propagated towards the symmetry plane and reflected as an *RR*.

Nozzle flow separation has been studied extensively over the past 50 years (Summerfield, Foster & Swan 1954; Reshotko & Tucker 1955; Morrisette & Goldberg 1978; Romine 1998; Nasuti, Onofri & Pietropaoli 2004) because of its importance to rocket engine performance. There are several models (empirical and analytical) (Uskov & Chernyshov 2006) to predict the onset of flow separation as a function of pressure

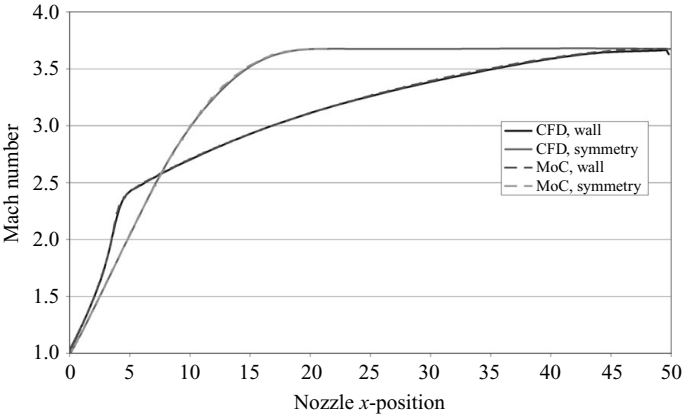

FIGURE 4. Mach number distribution along the symmetry plane and the nozzle wall for an ideal nozzle: dashed lines, MoC calculation; solid lines, CFD computation.

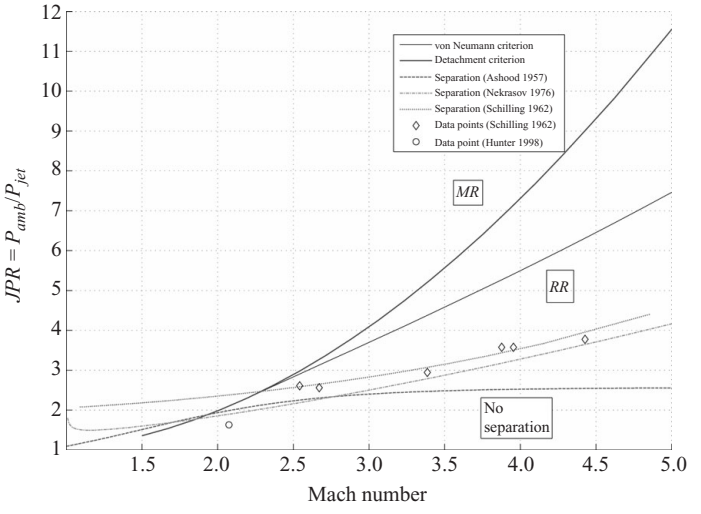

FIGURE 5. Flow separation pressure ratio criteria as functions of Mach number: dashed lines, flow-separation criteria (three models); solid lines, von Neumann criterion for *MR* and detachment criterion for *RR*; symbols, experimental data.

ratio. The work of Frey (2001) has an extensive review of flow-separation models that show that in the Mach number range of 2.5–4.5 the agreement with experimental results is good. Most of the empirical predictions are for axisymmetric nozzles, and the ones that are for planar nozzles are mainly for conical (constant angle) configuration (Hunter 1998). It is still possible to use the predictions developed for axisymmetric nozzles for planar ones because in both cases separation at the wall is primarily driven by the balance between the momentum of the supersonic jet and the static back pressure. Thus, for different Mach numbers, the separation will be initiated at different ratios of stagnation to ambient pressure. Plotting the critical pressure ratio, which initiates separation as a function of Mach number from several models, shows that for all Mach numbers greater than about 2.2 flow separation will occur below the dual-solution domain (figure 5). This means that as the pressure ratio increases from

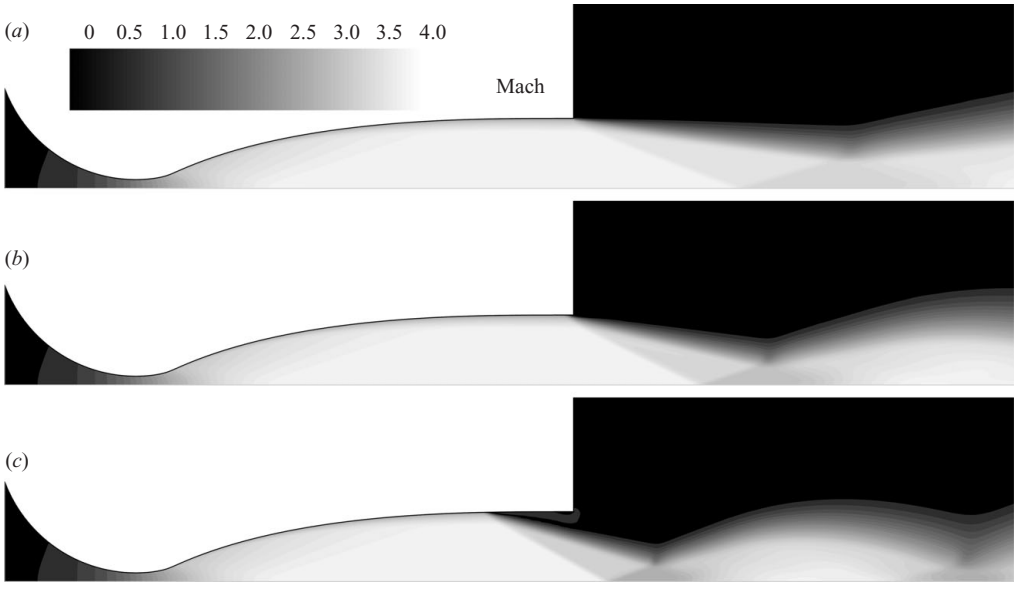

FIGURE 6. Mach contours of ideal nozzle at different pressure ratios, viscous simulation and $M_{jet} = 3.62$: (*a*) $JPR = 2$, no separation; (*b*) $JPR = 3$, start of separation; (*c*) $JPR = 4$, clear flow separation.

perfectly expanded to overexpanded conditions, flow separation will initiate before the transition from *RR* to *MR*. As the pressure ratio increases, the separation point will move upstream along the nozzle wall, and thus the whole shock system will move back into the nozzle, but the general flow structure will remain the same.

Numerical simulation of the nozzle at different jet-pressure ratios shows that the predictions of Schiling (1962) and Nekrasov, which appears in Abramovich (1976) are in good agreement with the resulting flow structure (figure 6). Although the nozzle contour was designed without making corrections for the boundary-layer growth, the flow at the outlet is uniform and parallel, but the Mach number is 3.62 instead of the designed Mach number of 3.67.

This result precludes the possibility of a shock-reflection hysteresis in the outlet of a planar nozzle because at Mach numbers below 2.2 the dual-solution domain reduces to null.

As seen in figure 6 the flow pattern of an *RR* followed by an interaction between the jet boundary and the reflected shock does not change when the flow starts to separate from the nozzle wall. The flow pattern shifts upstream, but the Mach number at the reflection point on the symmetry plane remains constant due to the fact that region downstream of the left-running characteristic from the symmetry plane to the nozzle outlet is a uniform region. As the *JPR* is increased the oblique shock becomes steeper, and the Mach number downstream of the *RR* approaches sonic conditions. The fact that the flow separation does not affect the reflection at the symmetry plane suggests that a transition from *RR* to *MR* is still possible at some pressure ratio.

2. Numeric method

Numerical simulation of flow separation in turbulent supersonic flow regime is a challenging task. The standard k–ε turbulence model is inadequate in predicting

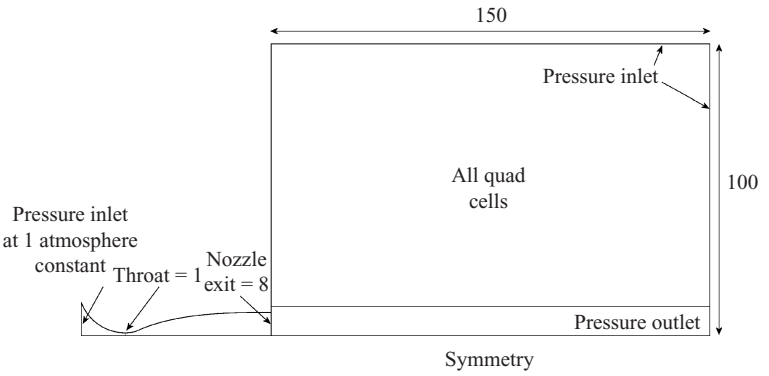

FIGURE 7. Computational domain with relative sizes and boundary conditions of the numerical simulation.

the separation point because of the adverse pressure gradients at the wall as well as the compressibility effect of the supersonic flow. For this reason, three variants of the two-equation model that are more suitable for such a flow were considered: the realizable model, the renormalization group (RNG) method k–ε model and the shear-stress-transport (SST) k–ω model (Speziale & Thangam 1992; Menter 1994; Mulvany *et al.* 2004).

In modelling boundary layers with CFD codes two different approaches can be used. In most cases, the boundary layer is not resolved down to the wall, and instead wall functions such as the universal wall law by Clauser (1956) are used. In this case, the cell height adjacent to the wall should be in the range $30 < y^+ < 150$ as defined by

$$y^+ \equiv \frac{yu_*}{\nu}; \quad u_* \equiv \sqrt{\frac{\tau_w}{\rho}}.$$

This approximation developed for incompressible flows may not be accurate for moderate Mach numbers such as the ones in the nozzle.

The second approach resolves the flow down to the laminar sublayer without the use of wall functions. In this case the cell height near the wall should be $y^+ \approx 1$. The first approach was used with the SST k-ω model and the second one with the realizable k–ε and RNG k–ε models.

The steady-state Reynolds-averaged Navier–Stokes equations were solved using the commercial finite-volume CFD program 'FLUENT', using a two-dimensional density-based implicit solver, with a second-order upwind discretization scheme. The computational domain was constructed with quadrilateral cells with special attention to the boundary layer and varying cell area according to the zones of interest. The nozzle zone was meshed densely, while the jet outside the nozzle and the ambient zone above it were gradually coarsened as the distance downstream and away from the symmetry line increased. The relative dimensions of the domain with the boundary conditions are presented in figure 7. Early simulations showed that the supersonic jet creates a suction effect, which draws fluid from the top and the right boundaries of the domain, and thus the boundary condition was set to 'pressure inlet' instead of 'pressure outlet'. In order to reduce the number of elements in the domain a symmetry boundary condition was imposed, and only the top part of the nozzle was modelled.

The simulation procedure was carried out in the following order. First, the pressure conditions at the outlet were set to produce flow without separation at a jet-pressure

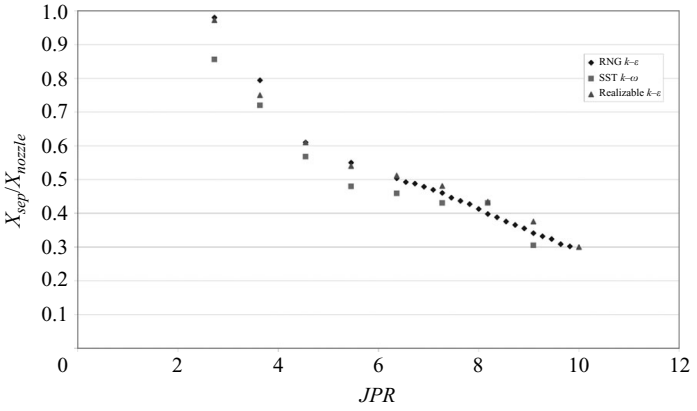

FIGURE 8. Location of separation point on the nozzle wall with different turbulent models.

ratio $JPR = 2$. The calculation was iterated until the residuals flattened and the mass balance was within a 2 % error margin. The pressure at the outlets was increased by $\Delta JPR = 1$ and calculated again until reaching $JPR = 7$; then the pressure increments were reduced to $\Delta JPR = 0.2$. At the end of each calculation the reflection type was checked until at $JPR = 11$ the reflection changed to *MR*. Then the pressure was decreased at the same increments until reaching $JPR = 7$. During the whole simulation, the pressure at the inlet of the nozzle was kept constant at 100 kPa, and thus the mass flow rate and the Reynolds number in the nozzle remained unchanged.

A grid convergence study was performed by using three mesh densities and observing the effect on the resulting flow pattern. The coarse grid consisted of ~15 000 cells in the divergent part of the nozzle and ~20 000 cells in the jet region. The average cell height in the nozzle was 1 % of the nozzle exit half-height. The medium grid consisted of ~60 000 and ~30 000 cells in the respective regions and a cell height of 0.25 % of the nozzle exit half-height. The fine grid consisted of ~183 000 and 120 000 cells respectively.

All grid densities gave essentially identical results except for the region of discontinuity in which the finer grids gave sharper change in properties. The transition between *RR* and *MR* in the coarse grid was at a lower pressure ratio than in the medium grid, but the change when using the fine grid was minimal. It was therefore decided to use the medium grid density for the rest of the simulation.

3. Results and discussion

3.1. *Viscosity model*

Of the three turbulent models tested the RNG k–ε model produced the best results. Although all the models gave similar predictions as to the location of the separation point on the wall of the nozzle as shown in figure 8, the realizable k–ε and SST k–ω models had problems with the turbulent viscosity ratio, which is the ratio of turbulent viscosity to molecular viscosity,

$$\beta = \frac{\nu_t}{\nu_m}.$$

In both models, the value of β had to be limited by the software to a value of 10 000 to prevent divergence of the solution.

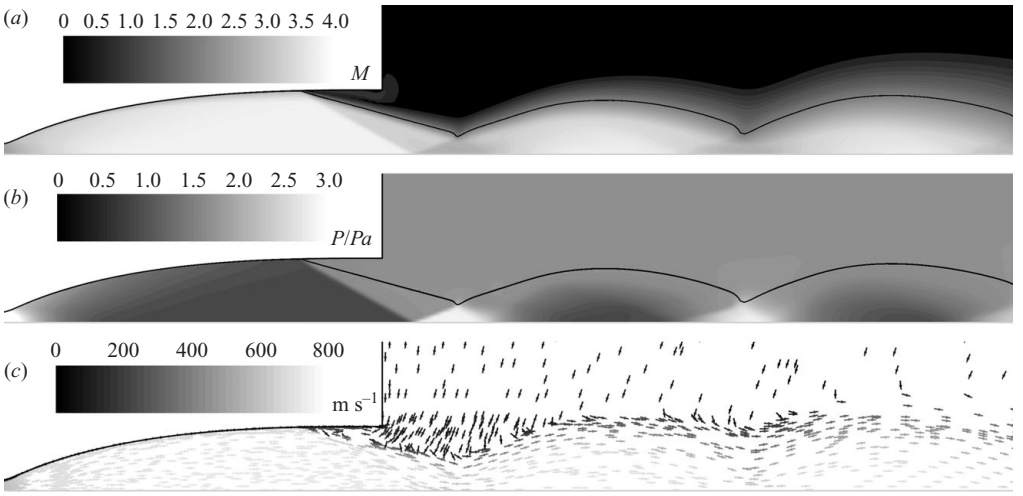

FIGURE 9. Typical flow structure of phase I pressure increase: (*a*) Mach number contours; (*b*) pressure contours normalized by ambient pressure; (*c*) velocity vectors (m s^{-1}); solid line, sonic line.

The SST k–ω model gave high values ($\beta \approx 5000$) in the separation area and yet higher values in the shear layer between the jet boundary and the jet core, while the supersonic region downstream of the incident shock wave showed low values ($\beta \approx 50$).

The realizable k–ε model gave high values ($\beta > 5000$) in the regions downstream of the incident shock wave, the reflected shock wave and the supersonic jet area (in the potential core of the jet in which the flow is assumed to be inviscid) while showing moderate values in the separated region ($\beta \approx 300$).

The RNG k–ε model resulted in high values ($\beta < 5000$) only near the pressure outlet boundary while showing moderate values ($\beta \approx 300$–1000) in the shear layer and in the separated area and low values in the jet core ($\beta < 20$).

For this reason, it was decided to perform the rest of the simulation with the RNG k–ε model.

3.2. *Flow structure on pressure increase*

3.2.1. *Phase I*

For $2 < JPR < 5$ (figure 9) a typical *RR* flow structure is formed consisting of a straight incident shock wave starting at the separation point and reflecting at the symmetry plane outside the nozzle. Downstream of the incident shock wave, a region of uniform Mach number with a velocity component parallel to the jet boundary and a pressure equal to that of the ambient is formed. Downstream of the reflected shock wave the flow is again parallel to the symmetry plane, while at the point where the reflected shock hits the jet boundary a centred expansion fan is formed, and the jet boundary is bent away from the symmetry plane. The reflection of the expansion fan from the symmetry plane and then from the jet boundary curves it again to form a dissipating, repeating wavy structure (shock cells) whose wavelength depends on the *JPR*. As the *JPR* increases, the reflection point moves upstream. It should be noted that the Mach number upstream of the incident shock wave is 3.61 and not 3.67 due to the effect of the boundary layer, which reduces the actual *AR* to 7.5.

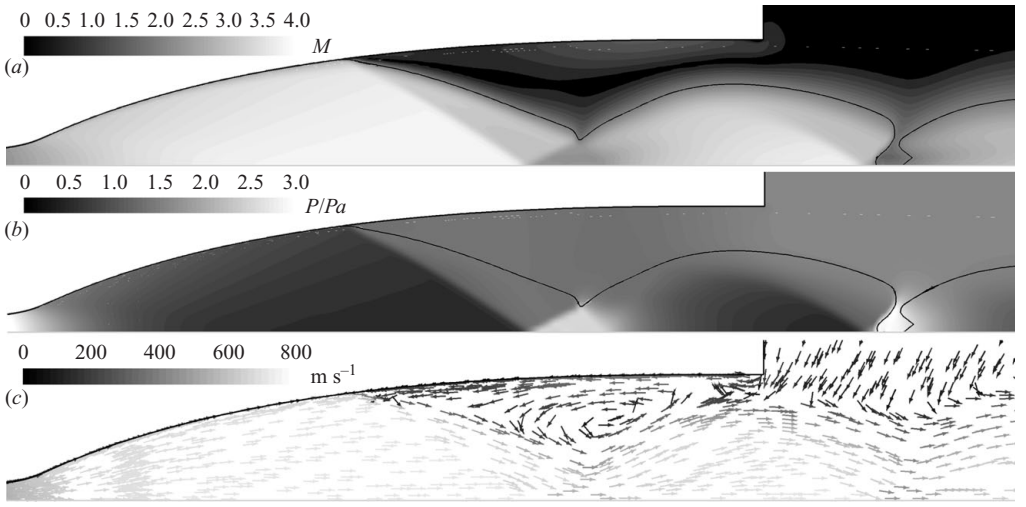

FIGURE 10. Typical flow structure of phase II pressure increase: (*a*) Mach number contours; (*b*) pressure contours; (*c*) velocity vectors; solid line, sonic line.

3.2.2. *Phase II*

For $5 < JPR < 8.4$ (figure 10) the point of separation shifts upstream to the extent that the reflection point is inside the nozzle. The incident shock wave is straight only downstream to the point at which the last left-running characteristic crosses the shock front; above this point the shock is bent because of the decreasing Mach number. A subsonic pocket develops downstream of the reflected shock wave between the first and second shock cells. As the ambient pressure increases, the subsonic pocket expands until it reaches the reflection point. The pressure downstream of the incident shock and above the jet boundary is lower than the ambient pressure; thus an upstream flow takes place, and a recirculation zone (termed separation bubble) develops. In the region between the jet and the wall, the total pressure starts to drop off at the nozzle exit plane and reaches its minimum value at the centre of the separation bubble, which is located above the point at which the jet boundary starts curving upwards.

3.2.3. *Phase III*

For $8.4 < JPR < 10$ (figure 11) the *RR* between the first and second shock cells abruptly transforms into an *MR*. Subsequent shock cells disappear, and instead a straight jet with a subsonic inner core develops. As the pressure ratio increases, the Mach-stem height diminishes as it moves upstream into the nozzle. The point of minimum total pressure in the recirculation zone moves upstream with the crest of the first shock cell, and a pressure gradient starts to develop between the incident shock wave and the jet boundary.

3.2.4. *Phase IV*

For $10 < JPR < 10.6$ (figure 12), the *MR* between the first and second shock cells reverts to *RR*, and the shock-cell structure downstream is re-established. A subsonic pocket develops in the region downstream of the first *RS*, and as the pressure increases it expands towards the reflection point. A second separation bubble appears between the first and second shock cells.

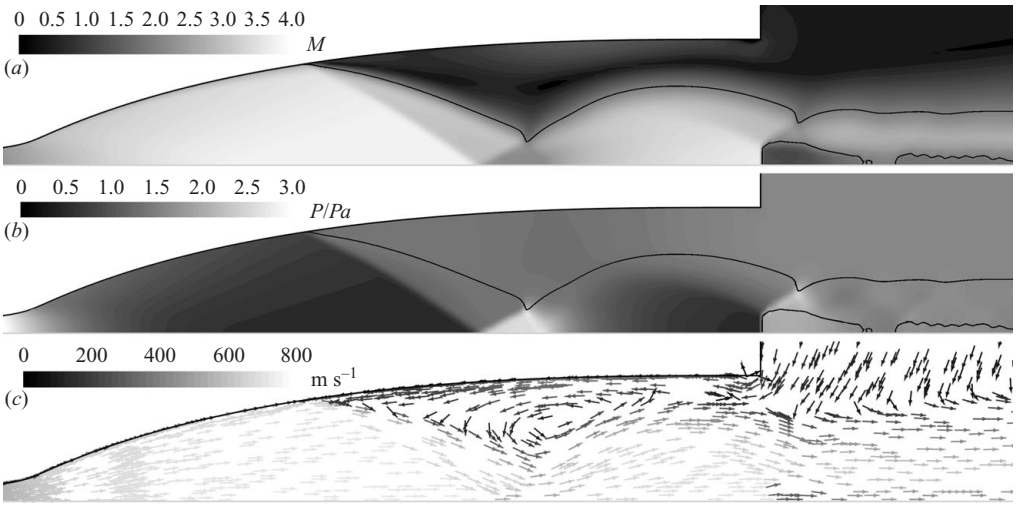

FIGURE 11. Typical flow structure of phase III pressure increase: (*a*) Mach number contours; (*b*) pressure contours; (*c*) velocity vectors; solid line, sonic line.

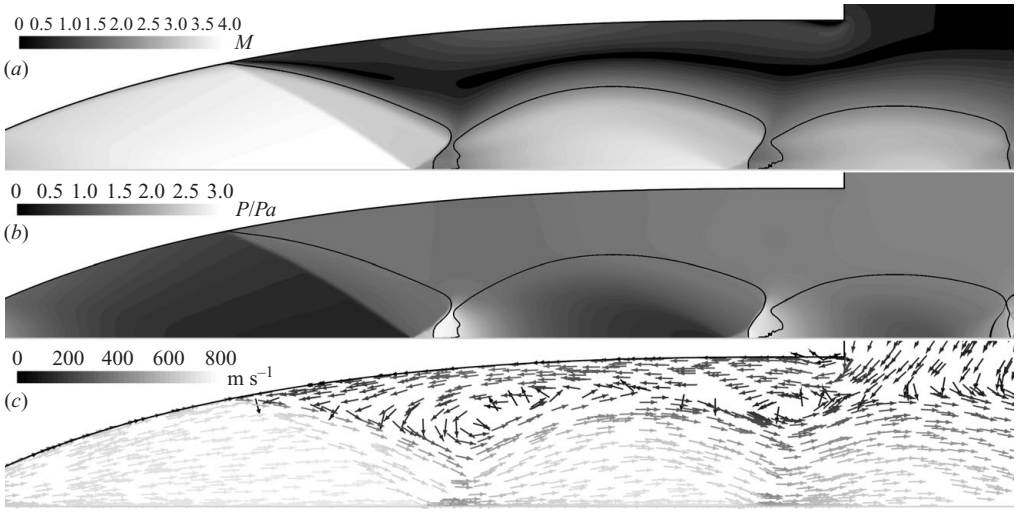

FIGURE 12. Typical flow structure of phase IV pressure increase: (*a*) Mach number contours; (*b*) pressure contours; velocity vectors; solid line, sonic line.

3.2.5. *Phase V*

For $JPR > 10.6$ (figure 13), the primary RR transforms into an MR, and subsequent shock cells disappear. The $RR \rightarrow MR$ transition takes place when the subsonic pocket reaches the reflection point; this suggests that the transition takes place at the sonic criterion. As the pressure increases, the Mach stem becomes larger. The pressure in the separated area is closer to the ambient value and more uniform. The separation bubbles unite into a prolonged one.

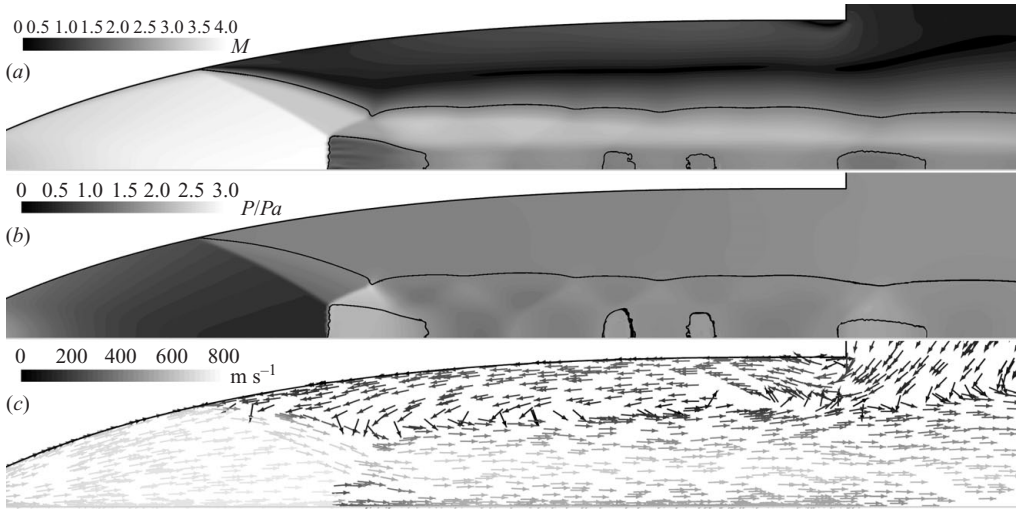

FIGURE 13. Typical flow structure of phase IV pressure increase: (*a*) Mach number contours; (*b*) pressure contours; (*c*) velocity vectors; solid line, sonic line.

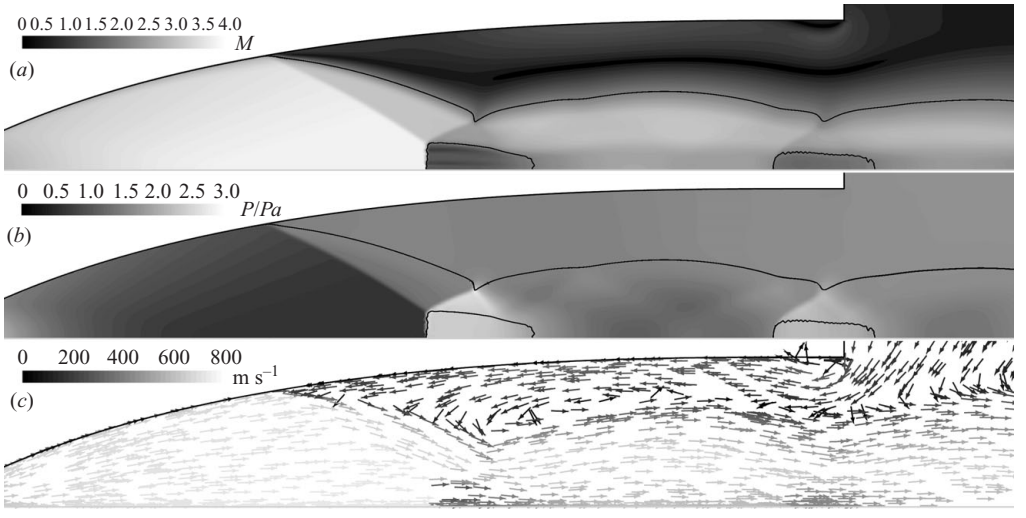

FIGURE 14. Typical flow structure of phase I pressure decrease: (*a*) Mach number contours; (*b*) pressure contours; (*c*) velocity vectors; solid line, sonic line.

3.3. *Flow structure on pressure decrease*

3.3.1. *Phase I*

For $JPR > 7.4$ (figure 14), a typical *MR* flow structure persists. It consists of a nearly perpendicular Mach stem and a triple point at which the *IS*, *RS*, *MS* and the slipstream connect. The slipstream is parallel to the symmetry plane, which suggests that the reflection is close to the von Neumann criterion. At the point at which the reflected shock hits the jet boundary, a centred expansion fan is formed, and the jet boundary is bent away from the symmetry plane. The expansion fan interacts with the slipstream, causing it to bend towards the symmetry plane and therefore accelerates the flow below it until it becomes supersonic. Downstream of the reflected

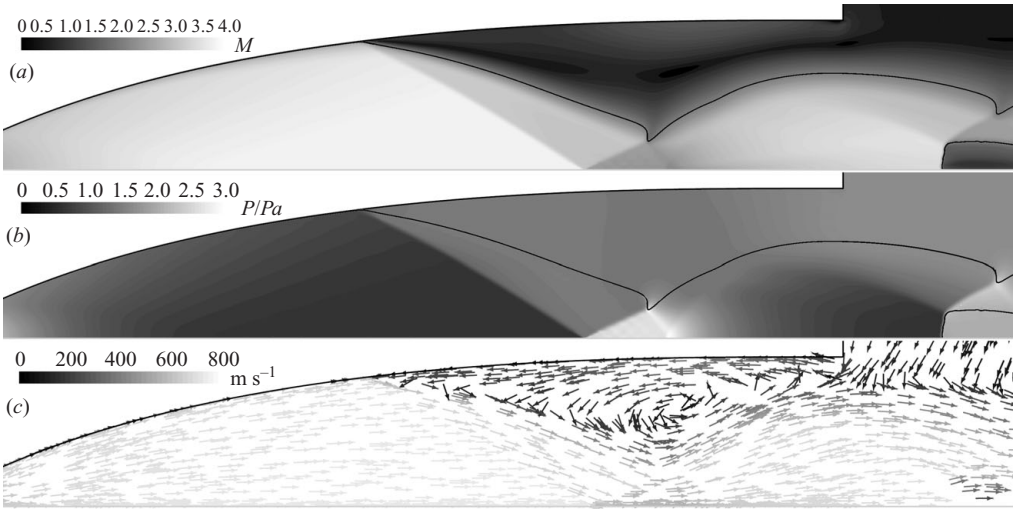

FIGURE 15. Typical flow structure of phase II pressure decrease: (*a*) Mach number contours; (*b*) pressure contours; (*c*) velocity vectors; solid line, sonic line.

shock wave and above the slipstream the flow is supersonic and accelerating when passing through the expansion fan. As the *JPR* is reduced the Mach stem decreases in size and moves downstream. Also, the jet boundary, which is almost straight at first, becomes increasingly wavier; accordingly the Mach number above and below the slipstream increases, and a shock-cell structure re-emerges. In each cell, the maximal Mach number is below the crest of the jet boundary. The Mach stem between the first and second shock cells, which is normal at the symmetry plane, bends downstream, as it departs from the symmetry plane because of the non-uniform conditions upstream of the shock wave.

3.3.2. *Phase II*

For $7.4 > JPR > 7.0$ (figure 15), the primary *MR* disappears, and the *RR* flow structure reappears. The reflection type between the first and second shock cells is an *MR* with the Mach stem getting smaller as the *JPR* is reduced.

3.3.3. *Phase III*

For $JPR < 7$, the flow structure is identical to the one observed during the pressure increase in phase I.

3.4. *Shock-polar analysis*

The driving force that determines the shock-wave angle ϕ the flow deflection angle θ and the Mach number downstream of the shock is the pressure ratio across it. When the primary shock reflection is outside the nozzle, this pressure ratio is equal to the *JPR*. This is because the shock is straight and the pressure downstream of the incident shock wave is equal to the ambient pressure, and so a pressure-deflection shock polar may be used to analyse it and predict at what pressure ratio the transition from *RR* to *MR* will occur.

However, when the primary reflection is inside the nozzle the pressure in the separated zone is not equal to the ambient pressure as Romine (1998) assumes in his analysis and thus cannot be analysed by shock polars. In order to overcome this problem two alternative pressure ratios were considered for use in a shock polar;

Pressure ratio	Detachment criterion	von Neumann criterion
Analytic	6.0	4.8
JPR	9.4–9.5	6.7–6.9
*AJPR*1	5.0–5.4	4.5–4.6
*AJPR*2	7.3–7.7	5.1–5.3
Average *AJPR*	6.35	4.88

TABLE 1. Comparison of analytic and computed transition criteria.

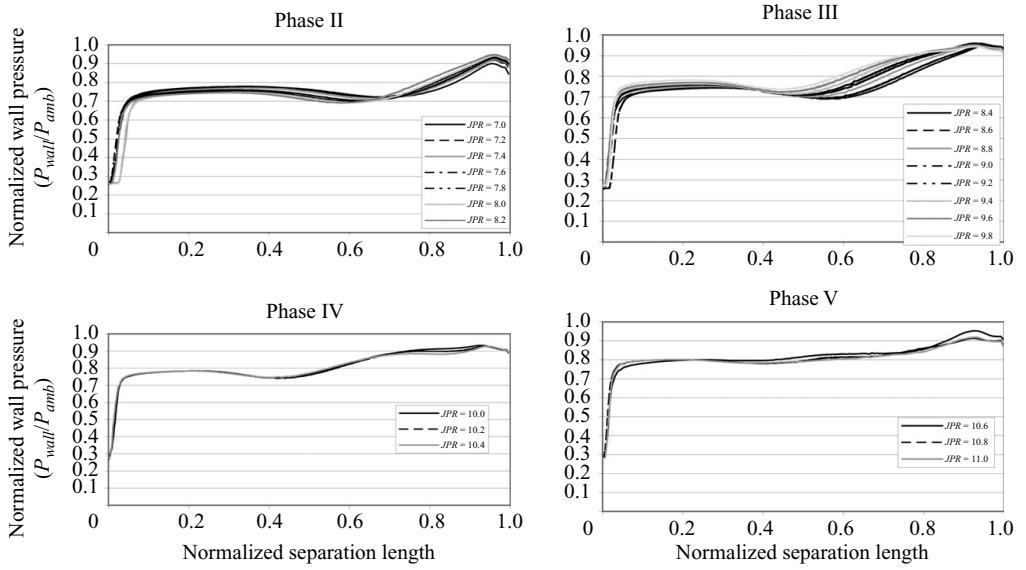

FIGURE 16. Normalized wall pressure from separation point to nozzle exit during pressure increase.

they are termed 'actual jet-pressure ratio' (*AJPR*). The first is the relation between the pressure just above the reflection point downstream of the incident shock wave and the jet pressure upstream of the incident shock wave (*AJPR*1). The second is the relation between the pressure at the jet boundary above the reflection point and the jet pressure (*AJPR*2); see points P_0, P_1 and P_2 in figure 1(*b*). A comparison of the analytic detachment and the von Neumann criteria to the proposed pressure ratios (Table 1) shows that none of them give satisfying results; *AJPR*1 underpredicts it, and *AJPR*2 overpredicts it. The average value of the two pressure ratios gives a reasonable agreement with the theoretical value.

3.5. *Pressure in the separated zone*

The assumption made in some previous works (Morrisette & Goldberg 1978; Hunter 1998; Romine 1998; Nasuti, Onofri & Pietropaoli 2004) that the pressure along the nozzle wall downstream of the separation point approaches the ambient pressure is found to be untrue for an ideal nozzle as noted by Lawrence & Weynand (1968). Frey (2001) noted the difference in pressure recovery between nozzles with small divergence angles (such as the ideal nozzle contour) and nozzles with large divergence angles (typical of rocket nozzles). Inspection of the pressure values along the nozzle wall from the point of separation towards the nozzle exit plane when the pressure is

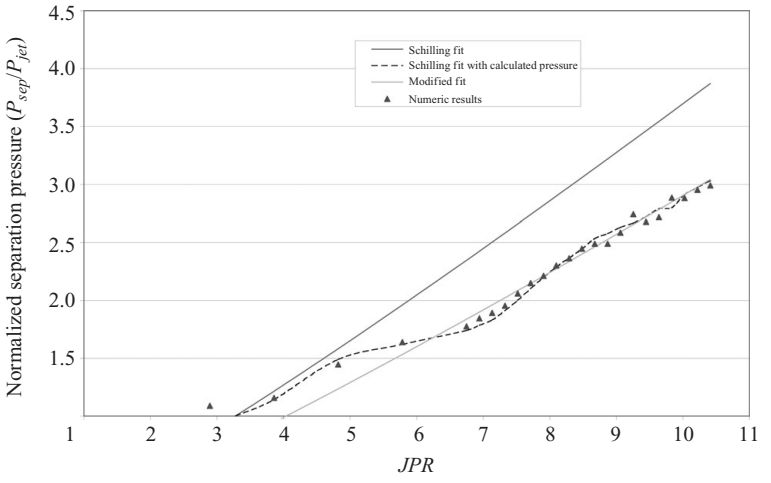

FIGURE 17. Non-dimensional separation pressure: lines, curve fits; symbols, numeric results.

increased shows a self-similar behaviour in each of the phases as shown in figure 16. The pressure increases abruptly across the separation point but does not recover to the ambient conditions, it remains in the range 70–80 % of the ambient pressure up to the nozzle exit. This pressure gradient promotes the backflow into the nozzle and the circulation bubble in the separated area. Another explanation for this effect is that when separation occurs inside the nozzle, the supersonic jet sucks ambient gas into the nozzle, with a stagnation pressure equal to ambient pressure. The ambient gas accelerates along the wall in a direction opposite to that of the main stream. As a result the static pressure along the wall, in the separated domain, decreases from the nozzle exit towards the separation point. However, this does not explain why the stagnation pressure in the separated area is at approximately the same value as the static pressure. When the transition to *MR* occurs (phase V) the pressure is nearly constant at 80 % of the ambient pressure. The similarity across different *JPR*s is kept on pressure decrease as well.

Schilling's curve fit relates the pressure just upstream of the separation point with the ambient and stagnation pressures:

$$P_{sep} = P_{amb} - C\,(P_0/P_{amb})^E\,,$$

where C and E are empirical constants, $C = 0.517$, $E = -0.913$.

When the calculated values are compared to the numeric results the agreement is good only for the onset of separation, but when the ambient pressure is replaced by the numerically calculated pressure downstream of the separation point, which is equal to the pressure above the jet boundary (P_2), the agreement is excellent (figure 17). Based on this result a modified curve fit is suggested for extensive separation:

$$P_{sep} = A P_{amb} - C\,(P_0/A P_{amb})^E\,,$$

where $A = 0.81$.

3.6. *Mach-stem height*

One of the measures of the hysteresis phenomenon in shock reflection is the height of the Mach stem. The precise dimensions of the Mach stem are difficult to deduce from numerical simulations because they depend on the local grid resolution and the

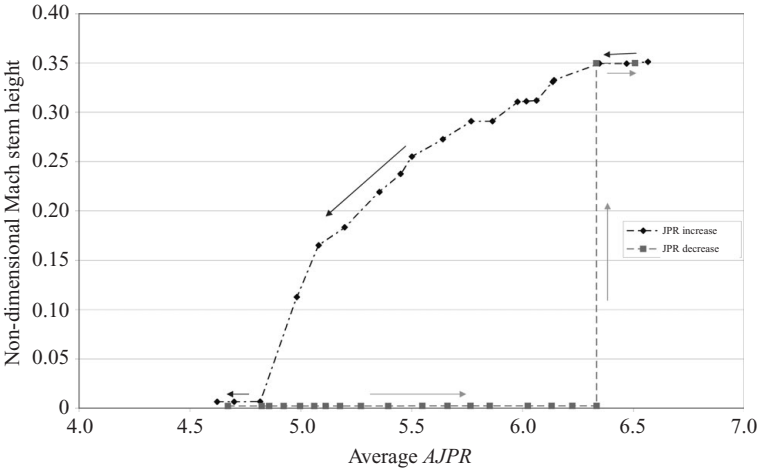

FIGURE 18. Non-dimensional Mach-stem height showing hysteresis loop on pressure increase and decrease.

threshold that determines the location at which the physical properties has changed. The method used in this work included two steps. In the first step, the reflection point on the symmetry plane was determined by measuring the location of the maximum strain-rate magnitude. Then the value of the y velocity component was measured along a line perpendicular to the symmetry plane at the reflection point, and the location was determined by setting a threshold value. Normalizing the height of the Mach stem is also ambiguous. According to Hornung *et al.* (1979), the Mach-stem height must have some physical length scale associated with it; in wedge flow it is usually the distance between the wedges or the wedge length, and in inviscid nozzle calculations, it is the nozzle exit height (Hadjadj 2004). In the case of separated flow, the equivalent non-dimensionalizing factor should be the nozzle height at the separation point. Figure 18 shows the hysteresis phenomenon in the Mach-stem height using the average value of $AJPR$.

4. Conclusion

A viscous numerical simulation of the shock-reflection transition in an overexpanded planar nozzle was conducted using the RNG method k–ε model. It was found that for all Mach numbers, boundary-layer separation will occur before the transition from RR to MR. Although models for predicting flow separation in a nozzle depend on the geometry of the nozzle wall, a modified version of the curve fit of Schilling (1962) is in good agreement with the numerical model.

Three versions of the two-equation turbulent Navier–Stokes computations were tested and showed similar results as to the relation between the ambient pressure and the location of the separation point, but the realizable k–ε model and the SST k–ω model resulted in unrealistic turbulent viscosity ratios in different flow regions.

The numerical simulation of the shock transition showed a complex behaviour in which the changing pressure ratio simultaneously affects the location of the separation point, the pressure ratio across the incident shock, the pressure in the separated flow area and the type of reflection. At first, the RR flow structure remains unchanged except for the movement upstream as the pressure ratio increases. Then an $RR \rightarrow MR$

transition occurs in the second shock cell, and only after it reverts to *RR* the transition in the primary incident shock takes place. For the same initial conditions on pressure decrease, the flow structure is different with an *MR* persisting until the Mach stem diminishes in size. The reflection mechanism is identical to the inviscid case in the sense that transition from *RR* to *MR* takes place when the subsonic pocket reaches the reflection point and the transition for *MR* to *RR* is at the von Neumann criterion.

The pressure on the wall downstream of the separation point is lower than the ambient pressure and has a self-similar behaviour for each phase of the flow. This reason, along with the curved shape of the incident shock, precludes the use of shock polars for the analysis of this type of reflection.

REFERENCES

Abramovich, G. N. 1976 Applied Gas Dyanamics. Nauka, Moscow.

Ashwood, P. F. & Crosse, G. W. 1957 The influence of pressure ratio and divergence angle on the shock position in two-dimensional, over-expanded, convergent-divergent nozzles. C.P. No. 327, British ARC.

Chpoun, A., Passerel, D., Li, H. & Ben-Dor, G. 1995 Reconsideration of oblique shock wave reflections in steady flows. Part 1. Experimental investigation. *J. Fluid Mech.* **301**, 19–35.

Clauser, F. H. 1956 The turbulent boundary layer. In *Advances in Applied Mechanics* (ed. H. L. Dryden, Th. von Karman & G. Kuerti), Academic.

Courant, R. & Friedrichs, K. O. 1948 *Supersonic Flow and Shock Waves*. Interscience.

Frey, M. 2001 Investigation of flow problems in rocket nozzles at overexpansion. PhD thesis, Institute of Aerodynamics and Gasdynamics, University of Stuttgart, Stuttgart, Germany.

Hadjadj, A. 2004 Numerical investigation of shock reflection phenomena in overexpanded supersonic jets. *AIAA J.* **42**, 570–577.

Hornung, H. G., Oertel, H. & Sandeman, R. J. 1979 Transition to Mach reflection of shock waves in steady and pseudosteady flow with and without relaxation. *J. Fluid Mech.* **90**, 541–560.

Hunter, C. A. 1998 Experimental, theoretical, and computational investigation of separated nozzle flows. In *Thirty-Fourth AIAA/ASME/SAE/ASEE Joint Propulsion Conference and Exhibit*, Cleveland, OH.

Ivanov, M. S., Vandromme, D., Fomin, V. M., Kudryavtsev, A. N., Hadjadj, A. & Khotyanovsky, D. V. 2001 Transition between regular and Mach reflection of shock waves: new numerical and experimental results. *Shock Waves* **11**, 99–107.

Kudryavtsev, A. N., Khotyanovsky, D. V., Hadjadj, A., Vandromme, D. & Ivanov, M. S. 2002 Numerical investigation of shock wave interactions in supersonic imperfectly expanded jets. In *Proceedings of the International Conference on Methods of Aerophysical Research*, 29 June 1998 – 3 July 1998, Akademiya Nauk SSSR Novosibirsk Inst Teoreticheskoi I Prikladnoi Mekhaniki, p. 138. See also:http://www.itam.nsc.ru/ENG/Conf/ICMAR/IR98/icmar98.html

Lawrence, R. A. & Weynand, E. E. 1968 Factors affecting flow separation in contoured supersonic nozzles. *AIAA J.* **6**, 1159–1160.

Li, H. & Ben-Dor, G. 1997 A parametric study of Mach reflection in steady flows. *J. Fluid Mech.* **341**, 101–125.

Menter, F. R. 1994 Two-equation eddy-viscosity turbulence models for engineering applications. *AIAA J.* **32**, 1598–1605.

Molder, S., Gulamhassein, A., Timofeev, E. & Voinovich, P. 1997 Focusing of conical shocks at the centreline of symmetry. In *Twenty-First International Symposium on Shock Waves*, Great Keppel Island, Australia.

Morrisette, E. L. & Goldberg, T. J. 1978 Turbulent-flow separation criteria for overexpanded supersonic nozzles. *Rep. No.* NASA-TP-1207, p. 40. NASA Langley Research Center.

Mulvany, N. J., Chen, L., Tu, J. Y. & Anderson, B. 2004 Steady-state evaluation of two-equation RANS (Reynolds-averaged Navier–Stokes) turbulence models for high-Reynolds number hydrodynamic flow simulations. *Sci. Lab. Rep. No.* DSTO-TR-1564, 66. DSTO.

Nasuti, F., Onofri, M. & Pietropaoli, E. 2004 The influence of nozzle shape on the shock structure in separated flows. In *Proceedings of the Fifth European Symposium Aerothermodynamics for Space Vehicles* 8–11 November 2004, Cologne, Germany. (ed. D. Danesy), p. 353.

von Neumann, J. 1943 Oblique reflection of shocks. In *John von Neumann's Collected Works* (ed. A. H. Taub), 1st edn., p. 238. Pergamon.

Ralov, A. I. 1990 On the impossibility of regular reflection of a steady-state shock wave from the axis of symmetry. *J. Appl. Math. Mech.* **54**, 200–203.

Reshotko, E. & Tucker, M. 1955 Effect of a discontinuity on turbulent boundary-layer-thickness parameters with application to shock-induced separation. *Rep. No.* TN 3454. NACA.

Romine, G. L. 1998 Nozzle flow separation. *AIAA J.* **36**, 1618–1625.

Schilling, M. 1962 Flow separation in a rocket nozzle. MS thesis, Graduate School of Arts and Sciences, University of Buffalo, Buffalo, NY.

Schotz, M., Levy, A., Ben-Dor, G. & Igra, O. 1997 Analytical prediction of the wave configuration size in steady flow Mach reflections. *Shock Waves* **7**, 363–372.

Shimshi, E., Ben-Dor, G. & Levy, A. 2008 Viscous simulation of shock reflection hysteresis in overexpanded planar nozzles. In *Eighteenth International Shock Interaction Symposium*, Rouen, France.

Sivells, J. C. 1978 A computer program for the aerodynamic design of axisymmetric and planar nozzles for supersonic and hypersonic wind tunnels. *Rep. No.* AEDC-TR-78-63. Arnold Engineering Development Center.

Skews, B. W. 1997 Aspect ratio effects in wind tunnel studies of shock wave reflection transition. *Shock Waves* **7**, 373–383.

Speziale, C. G. & Thangam, S. 1992 Analysis of an RNG based turbulence model for separated flows. *Intl J. Engng Sci.* **30**, 1379–1388.

Summerfield, M., Foster, C. R. & Swan, W. C. 1954 Flow separation in overexpanded supersonic exhaust nozzles. *Jet Propul.* **24**, 319–321.

Uskov, V. N. & Chernyshov, M. V. 2006 Differential characteristics of the flow field in a plane overexpanded jet in the vicinity of the nozzle lip. *J. Appl. Mech. Tech. Phys.* **47**, 366–376.

Vuillon, J., Zeitoun, D. & Ben-Dor, G. 1995 Reconsideration of oblique shock wave reflections in steady flows. Part 2. Numerical investigation. *J. Fluid Mech.* **301**, 37–50.